Eur. Phys. J. C 32, 535–546 (2004)
Digital Object Identifier (DOI) 10.1140/epjc/s2003-01443-6

THE EUROPEAN PHYSICAL JOURNAL C

Correlations between multiplicities and average transverse momentum in the percolating color strings approach

M.A. Braun[1,2], R.S. Kolevatov[1], C. Pajares[2], V.V. Vechernin[1]

[1] Department of High-Energy Physics, S. Petersburg University, 198504 S. Petersburg, Russia
[2] Department of Particle Physics, University of Santiago de Compostela, 15704 Santiago de Compostela, Spain

Received: 4 July 2003 / Revised version: 12 September 2003 /
Published online: 18 December 2003 –

Abstract. Long range multiplicity–multiplicity, p_{T}^2–multiplicity and p_{T}^2–p_{T}^2 correlations are studied in the percolating color string picture under different assumptions of the dynamics of the string interaction. It is found that the strength of these correlations is rather insensitive to these assumptions; nor is it sensitive to the geometry of the fused string clusters that formed, the percolation phase transition in particular. Both multiplicity–multiplicity and p_{T}^2–multiplicity correlations are found to scale and depend only on the string density. p_{T}^2–multiplicity correlations, which are absent in the independent string picture, are found to be of the order of 10% for central heavy ion collisions and can serve as a clear signature of string fusion. In contrast p_{T}^2–p_{T}^2 correlations turned out to be inversely proportional to the number of strings and therefore to be very small for realistic collisions.

1 Introduction

The standard description of particle production in soft high-energy strong interactions is in terms of color strings stretched between the participant hadrons, whose decay generates the observed particle spectrum. The number of strings grows with energy and atomic number of participants and reaches thousands in heavy ion collision at RHIC and LHC energies. With their density high enough, one expects that the strings begin to overlap and interact. Some time ago a scenario of this interaction was introduced based on the percolation phase transition and the existence of color strings of high color [1]. An immediate consequence of the percolating string scenario is damping of the multiplicity and rising of the average transverse momentum as compared to the independent string picture. These consequences are in agreement with the first data obtained at RHIC [2]. It is to be stressed that within the percolating string scenario one may imagine different versions of the string interaction dynamics. Overlapping strings may not interact at all. Then the consequence of overlapping will be just formation of different spots in the interaction area with higher color content corresponding to the sum of colors of the overlapping strings. These spots will generally act as independent particle emitters ("overlaps", or "ministrings"). The number of ministrings will generally be much greater than that of the initial strings. So in this scenario percolation and fusion of strings actually leads to a proliferation of particle emitters. An opposite scenario with a lot of interaction of overlapping strings assumes that their color becomes homogeneously distributed over the formed cluster, the latter as a whole becoming an independent particle emitter. In this scenario the number of particle emitters is evidently smaller than the number of initial strings and may become unity if all strings form a single cluster. It is remarkable that these two scenarios actually lead to practically the same predictions for such global quantities as the multiplicity and average transverse momentum. So, to distinguish between them, one has to study more detailed information of the particle spectra. Immediate candidates are the long range correlations between multiplicities or multiplicities and average transverse momentum. In this note we study these observables in both discussed scenarios of the string interaction. Our results show that unfortunately these long range correlations are not very sensitive to the choice of string dynamics either. In fact, we find that they are also rather insensitive to the geometric picture of the string fusion and to the percolation phase transition which occurs at high enough string density.

However, there is one advantage of studying the long range correlations involving the average transverse momenta: these correlations are absent in the independent string model. So their presence is a clear signature of string fusion and appearance of spots with higher color density than on the average. As we shall see, the correlations between the transverse momentum and multiplicity are of especial value, since they depend only on the string density and not on the total number of strings. Long range correlations between transverse momenta, on the contrary, are inversely proportional to the total number of strings

and so are practically absent in central heavy ion collisions. They can only be expected to be visible in highly peripheral collisions or collisions involving light nuclei.

Some comments are to be made to explain the application of the color string approach to correlations. First we shall study long range correlations, which correspond to choosing the correlating observables from different rapidity windows separated by a reasonably large rapidity interval. This is to exclude short range correlations which are always present and appear both at the string decay stage (internal correlations of string particle production) and final hadronization stage (resonance decays). Second, in the study of average transverse momentum we assume the chosen rapidity windows to exclude the fragmentation regions, where the correlations between the average transverse momentum and multiplicities may largely be a result of summing the transverse momenta of the parent partons from the colliding hadrons. In fact the latter explanation is the standard one for the observed correlations [3]. However it does not apply to the central region, in which particle production becomes insensitive to the parent parton momenta. So, hopefully the correlations in the central region result only due to string interactions. Finally we have to remember that the unperturbative color string picture is mostly oriented to soft particle spectra. Therefore, strictly speaking, our region of average transverse momenta should be limited by values of the order of $1 \div 2\,\mathrm{GeV}/c$. Nevertheless one may try to include also the lower part of the hard spectrum into the string mechanism of particle production, choosing the p_T distribution for a single string appropriately. Clustering of strings then suppresses the high p_T distributions in central heavy ion collisions in agreement with the RHIC data [2]. This seems to support the applicability of the string picture up to values of p_T of the order $8 \div 10\,\mathrm{GeV}/c$.

2 General formalism

In this subsection we shall present our basic probabilistic expressions for the correlations valid for any scenario of string interaction.

In a given event color strings occupy certain regions in the transverse interaction plane and may overlap forming clusters. In any scenario this generates independent emitters, either overlaps or clusters as a whole. We enumerate these emitters by the subindex $\alpha = 1, 2, 3, \ldots, M$, where M is the total number of emitters.

An event consists of the emission of m_α particles from emitter α. The total number of emitted particles is

$$m_\mathrm{e} = \sum_\alpha m_\alpha \,. \tag{1}$$

The p_T distribution of particles emitted from emitter α will be given by a certain function $w_\alpha(p)$. Note that it corresponds to the average

$$p_\alpha^2 = \int \mathrm{d}^2 p p^2 w_\alpha(p) \,, \tag{2}$$

whose concrete value depends of the scenario for the interaction. The effective p_T distribution in a given event is then

$$w_\mathrm{e}(p) = \frac{1}{m_\mathrm{e}} \sum_\alpha m_\alpha w_\alpha(p) \,, \tag{3}$$

and the average p_T^2 is

$$p_\mathrm{e}^2 = \frac{1}{m_\mathrm{e}} \sum_\alpha m_\alpha p_\alpha^2 \,. \tag{4}$$

Now we pass to taking averages over many events. This averaging may be divided in two steps. First we average over various events occurring with the same string geometry, that is, with the fixed overlap and cluster structure ("configuration"). Then we have to average over all possible configurations.

To average over events at a fixed configuration we have to know the probability $\rho_\alpha(m)$ for a given emitter to produce m particles. This probability has to lead to the average number of particles

$$\bar{m}_\alpha = \sum_m m \rho_\alpha(m) \,, \tag{5}$$

which again is to be taken according to the chosen scenario of the string interaction. We get averages in a given configuration:

$$\bar{m}_c = \sum_{\{m_\alpha\}} \prod_\alpha \rho_\alpha(m_\alpha) m_\mathrm{e} = \sum_\alpha \bar{m}_\alpha \,, \tag{6}$$

$$\bar{p^2}_c = \sum_{\{m_\alpha\}} \prod_\alpha \rho_\alpha(m_\alpha) \frac{1}{m_\mathrm{e}} \sum_\alpha m_\alpha p_\alpha^2 \tag{7}$$

and also the probabilities in a given configuration to emit m particles

$$\rho_c(m) = \sum_{\{m_\alpha\}} \prod_\alpha \rho_\alpha(m_\alpha) \delta_{m, \sum_\alpha m_\alpha} \tag{8}$$

and a particle with the transverse momentum p

$$w_c(p) = \sum_{\{m_\alpha\}} \prod_\alpha \rho_\alpha(m_\alpha) \frac{\sum_\alpha m_\alpha w_\alpha(p)}{\sum_\alpha m_\alpha} \,. \tag{9}$$

To study correlations we have to know double distributions. As mentioned in the introduction, we assume that the forward and backward rapidity windows are separated by a rapidity gap of sufficient length to exclude short range correlations. Then emissions into the forward and backward rapidity windows can be considered to be independent. As a result the double distribution in the numbers of particles m_F and m_B emitted in the forward and backward rapidity windows in a given configuration factorizes:

$$\rho_c(m_\mathrm{F}, m_\mathrm{B}) = \rho_c^\mathrm{F}(m_\mathrm{F}) \rho_c^B(m_\mathrm{B}) \,, \tag{10}$$

where the $\rho_c^{\mathrm{F,B}}(m)$ are given by (8) with emitter probabilities $\rho_\alpha^{\mathrm{F,B}}(m)$ to produce particles in the forward (F)

or backward (B) rapidity windows. Similarly the double distribution in the number of particles $m_{\rm F}$ in the forward rapidity window and the particle transverse momentum $p_{\rm B}$ in the backward rapidity window in a given configuration is a product:

$$\rho_c(m_{\rm F},p_{\rm B})=\rho_c^{\rm F}(m_{\rm F})w_c^{\rm B}(p_{\rm B})\,. \tag{11}$$

Here $w^{\rm B}(p)$ is given by (9) with $\rho_\alpha\to\rho_\alpha^{\rm B}$. Finally, the double distribution in the momenta $p_{\rm F}$ and $p_{\rm B}$ of the particles emitted in the forward and backward rapidity windows factorizes as follows:

$$w_c(p_{\rm F},p_{\rm B})=w_c^{\rm F}(p_{\rm F})w_c^{\rm B}(p_{\rm B})\,. \tag{12}$$

To average over different configurations we have to sum these expressions over all configurations with the weight P_c, which is the probability of a given configuration. We denote this operation as $\langle\ \rangle$. In particular we find various conditional probabilities of interest. The conditional probability to find $m_{\rm B}$ particles in the backward rapidity window provided one sees $m_{\rm F}$ particles in the forward rapidity window is

$$\langle\rho(m_{\rm B})\rangle_{m_{\rm F}}=\frac{\langle\rho_c(m_{\rm F},m_{\rm B})\rangle}{\langle\rho_c^{\rm F}(m_{\rm F})\rangle}\,. \tag{13}$$

The conditional probability to find a particle with transverse momentum $p_{\rm B}$ in the backward rapidity window provided one sees $m_{\rm F}$ particles in the forward rapidity window is

$$\langle w(p_{\rm B})\rangle_{m_{\rm F}}=\frac{\langle\rho_c(m_{\rm F},p_{\rm B})\rangle}{\langle\rho_c^{\rm F}(m_{\rm F})\rangle}\,. \tag{14}$$

Finally, the conditional probability to find a particle with momentum $p_{\rm B}$ in the backward rapidity window provided one sees a particle with momentum $p_{\rm F}$ in the forward rapidity window is

$$\langle w(p_{\rm B})\rangle_{p_{\rm F}}=\frac{\langle w_c(p_{\rm F},p_{\rm B})\rangle}{\langle w_c^{\rm F}(p_{\rm F})\rangle}\,. \tag{15}$$

Taking the averages with these probabilities we find our basic formulas for the correlations. The average multiplicity in the backward window at a given multiplicity in the forward window is

$$\langle m_{\rm B}\rangle_{m_{\rm F}}=\frac{\langle(\bar m_{\rm B})_c\rho_c^{\rm F}(m_{\rm F})\rangle}{\langle\rho_c^{\rm F}(m_{\rm F})\rangle}\,, \tag{16}$$

where $(\bar m_{\rm B})_c$ and $\rho_c^{\rm F}(m_{\rm F})$ are given by (6) and (8) for the two rapidity windows. The average transverse momentum squared in some rapidity window at a given multiplicity in a different rapidity window is

$$\langle {p_{\rm B}}^2\rangle_{m_{\rm F}}=\frac{\langle(\bar{p_{\rm B}^2})_c\rho_c^{\rm F}(m_{\rm F})\rangle}{\langle\rho_c^{\rm F}(m_{\rm F})\rangle}\,, \tag{17}$$

where $(\bar{p_{\rm B}^2})_c$ is given by (7) with $\rho_\alpha\to\rho_\alpha^{\rm B}$. Finally, the average transverse momentum squared in some rapidity window at a given momentum in a different rapidity window is

$$\langle {p_{\rm B}}^2\rangle_{p_{\rm F}}=\frac{\langle(\bar{p_{\rm B}^2})_c w_c^{\rm F}(p_{\rm F})\rangle}{\langle w_c^{\rm F}(p_{\rm F})\rangle}\,, \tag{18}$$

where $w_c^{\rm F}$ is given by (9) with $\rho_\alpha\to\rho_\alpha^{\rm F}$. These formulas serve as a starting point for our study.

The expressions for the correlations can be substantially simplified if the emission probabilities $\rho_\alpha(m)$ have the Poisson form

$$\rho_\alpha(m)=P_{\bar m_\alpha}(m)=\mathrm{e}^{-\bar m_\alpha}\frac{\bar m_\alpha^m}{m!}\,. \tag{19}$$

Then taking the average in a given configuration can be done analytically.

In particular we find with (19) (see Appendix A)

$$\rho_c(m)=P_{\bar m_c}(m)=\mathrm{e}^{-\bar m_c}\frac{\bar m_c^m}{m!}\,, \tag{20}$$

$$\bar{p^2}_c=\frac{1}{\bar m_c}\sum_\alpha\bar m_\alpha p_\alpha^2 \tag{21}$$

and

$$w_c(p)=\frac{1}{\bar m_c}\sum_\alpha\bar m_\alpha w_\alpha(p)\,. \tag{22}$$

For particles emitted in the forward (backward) rapidity windows one has to substitute in these formulas $\bar m\to\bar m_{\rm F,B}$

With this simplification, calculation of the correlations reduces to taking the averages only over configurations.

3 Multiplicity correlations

Forward–backward (FB) correlations between multiplicities have since long ago been studied both experimentally [4] and theoretically [5–7]. On the theoretical level they demonstrate that the number of elementary emitters fluctuates. On this ground they have served as a confirmation of the color string picture, showing that the number of strings fluctuates, with its average growing with energy. For the FB multiplicity correlations to exist, the interaction between strings is irrelevant: the correlations are fully present when strings are independent. Moreover, as conjectured in [8], interaction and fusion of strings lead to damping of these correlations, since the effective number of strings diminishes. As we shall see, this conjecture is confirmed by calculations using (16) in any of the two scenarios for the string interaction.

3.1 Ministrings as emitters

As mentioned in the Introduction the two scenarios differ in the intensity of the interaction between the overlapping strings. The ministring scenario assumes that this interaction is in fact absent: the overlap regions retain their form and serve as independent emitters of particle with characteristics determined by the total color accumulated in the

overlap. In this scenario different emitters can be labeled by two numbers $\alpha = \{ni\}$ where $i = 1, 2, \ldots$ enumerates the overlaps of n strings. The basic quantity which characterizes the ministring scenario is the average multiplicity of overlap $\{ni\}$ [1,8]:

$$\bar{m}_{ni} = \mu_0 \sqrt{n} \frac{S_{ni}}{\sigma_0} \,. \tag{23}$$

Here S_{ni} and σ_0 are transverse areas of the overlap and initial string, respectively. Using (6) we obtain the average multiplicity in a given configuration as

$$\bar{m}_c = \mu_0 \sum_n \sqrt{n} \frac{S_n}{\sigma_0} \,, \tag{24}$$

where $S_n = \sum_i S_{ni}$ is the total area in which n strings overlap, and μ_0 is the average multiplicity for the initial string. The average multiplicities in the forward and backward rapidity windows are given by the same formula with $\mu_0 \to \mu_0^{\mathrm{F,B}}$, the forward and backward multiplicities for the initial string:

$$\bar{m}_c^{\mathrm{F,B}} = \mu_0^{\mathrm{F,B}} \sum_n \sqrt{n} \frac{S_n}{\sigma_0} \,. \tag{25}$$

Putting (25) into (20) and using (16) we reduce the calculation of the FB multiplicity correlations to averaging over the overlap geometries of the known expression depending on S_n. This averaging involves, first, different ways in which string overlap with their total N number fixed and, second, different values of N distributed around a certain average value $\langle N \rangle$ determined by the energy and atomic number of participants. At large $\langle N \rangle$ and small σ_0 as compared to the total interaction area S one expects a scaling behavior: appropriately chosen characteristics of the correlations depend only on the dimensionless percolation parameter

$$\eta = \frac{\langle N \rangle \sigma_0}{S} \,. \tag{26}$$

This property allows one to study the correlations by Monte Carlo simulations with comparatively low values of $\langle N \rangle$. Values of η and $\langle N \rangle$ for S–S and Pb–Pb central collisions at different energies obtained by Monte Carlo simulations based on the fusing color string model [1] are shown in Table 1[1]. We have taken $\sigma_0 = \pi r_0^2$ with $r_0 = 0.2\,\mathrm{fm}$ and $S = \pi R_A^2$, which corresponds to central collisions ($b = 0$). Note that η defined by (26) is just a parameter describing the overall averages. In different events the number of particles fluctuates and so does the string density. One then may introduce η_{e} for a given event. However it is remarkable that the final averages as a result are found to be dependent only on the average η. In our numerical calculations we studied the quantity

$$F_{\mu-\mu} = \frac{\langle m_{\mathrm{B}} \rangle_{m_{\mathrm{F}}}}{\langle m_{\mathrm{B}} \rangle} - 1 \tag{27}$$

[1] These values are somewhat different from the ones previously used in [8], where they were computed from the naive Glauber–Gribov approach, in the optical approximation for AA collisions and without taking into account energy-momentum conservation.

Table 1. Values of η and average number of strings $\langle N \rangle$ for central S–S and Pb–Pb collisions at different energies

S–S scattering ($b = 0$)			Pb–Pb scattering ($b = 0$)		
$\sqrt{s}$	η	$\langle N \rangle$	$\sqrt{s}$	η	$\langle N \rangle$
19.4	0.40	126	19.4	1.08	1190
62.5	0.52	164	62.5	1.39	1536
200	0.65	204	200.0	1.60	1800
546	0.80	252	546.0	2.03	2240
1800	0.97	308	1800.0	2.46	2720
5500	1.19	378	5500.0	3.01	3329

as a function of

$$x = \frac{m_{\mathrm{F}}}{\langle m_{\mathrm{F}} \rangle} \,. \tag{28}$$

In our simulations we used both the homogeneous distribution of strings in the transverse interaction area and the inhomogeneous one, which follows the nuclear profile function $T(b)$. No significant qualitative difference was found between these two choices. For simplicity we present here our results for the homogeneous distribution. We chose $\mu_0^{\mathrm{F,B}} = 1$. We used the Poisson distribution in the number of strings N with $\langle N \rangle = 25$ and 50. We have checked that the results are practically independent of $\langle N \rangle$ in the region $0.3 < x < 3$, so that $F_{\mu-\mu}(x)$ exhibits the expected scaling behavior for physically relevant values of m_{F}.

Our results for values of $\eta = 0.5 \div 3$ show that in the whole interval $0 < x < 3$ the $F_{\mu-\mu}(x)$ is a monotonically rising function of x, rather close to linear and crossing zero at $x = 1$. Its slope at $x = 1$ (and $\langle N \rangle = 50$) (the "correlation coefficient")

$$b_{\mu-\mu} = \left(\frac{\mathrm{d}F_{\mu-\mu}(x)}{\mathrm{d}x} \right)_{x=1}$$

is shown in Fig. 1 by a solid line. As we observe, it steadily falls with η, in full accordance with the idea that the correlations are diminished as a consequence of string fusion. At very high η the slope seems to flatten around 0.1. At $\eta \to 0$ the slope tends to the value 0.5, which corresponds to the independent string model with the assumed value of μ_0 (see Appendix B). Note that $\eta \sim 1.12$ corresponds to the critical value for the percolation phase transition for the homogeneous distribution of strings (see [9] for the inhomogeneous case).

However, our curves do not show any peculiarity at such values of η.

In Fig. 2 we compare $b_{\mu-\mu}$ for the homogeneous distribution of strings and the inhomogeneous one which follows the nuclear profile function $T(b) \propto \sqrt{R_A^2 - b^2}$ (corresponding to a constant nuclear density). As mentioned, the difference is of no practical importance.

One may wonder why in the ministring case, with the proliferation of individual emitters, the multiplicity correlations are diminished, contrary to the common belief that they grow with the number of emitters [3]. The reason is that for multiplicities the effective emitters are not individual ministrings but rather the whole set of them with a

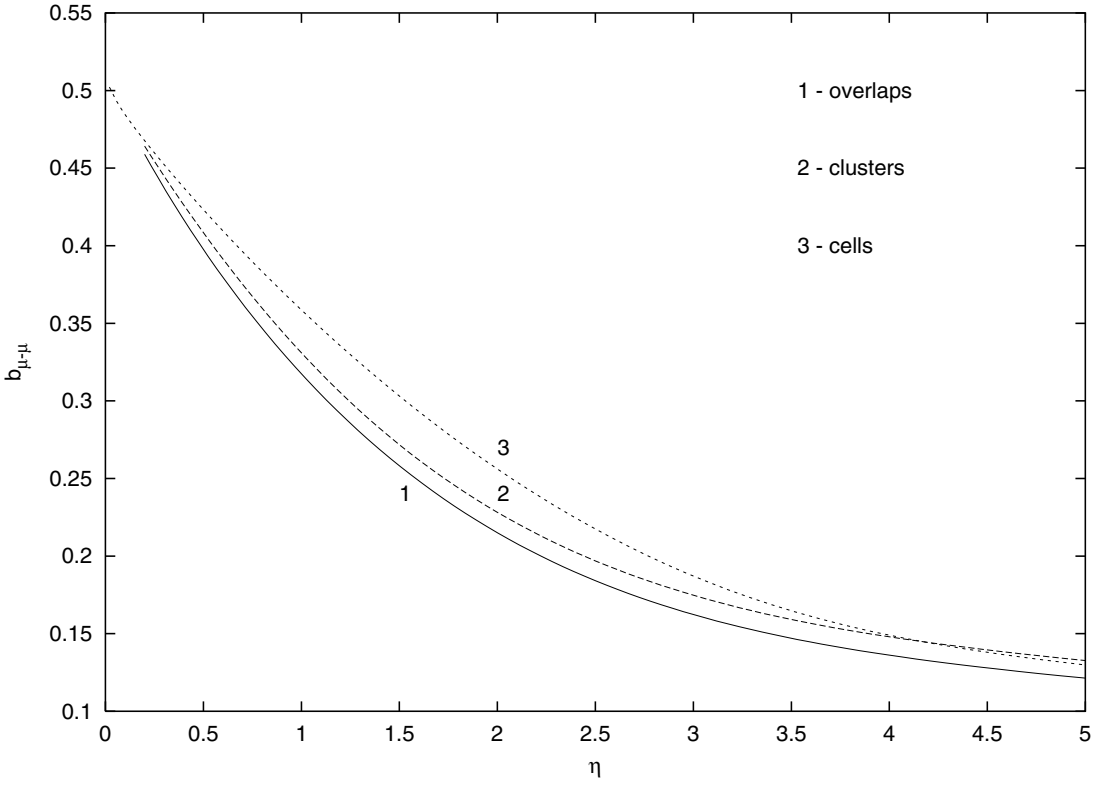

Fig. 1. Correlation coefficient $b_{\mu-\mu}$ for μ–μ correlations in the three scenarios studied

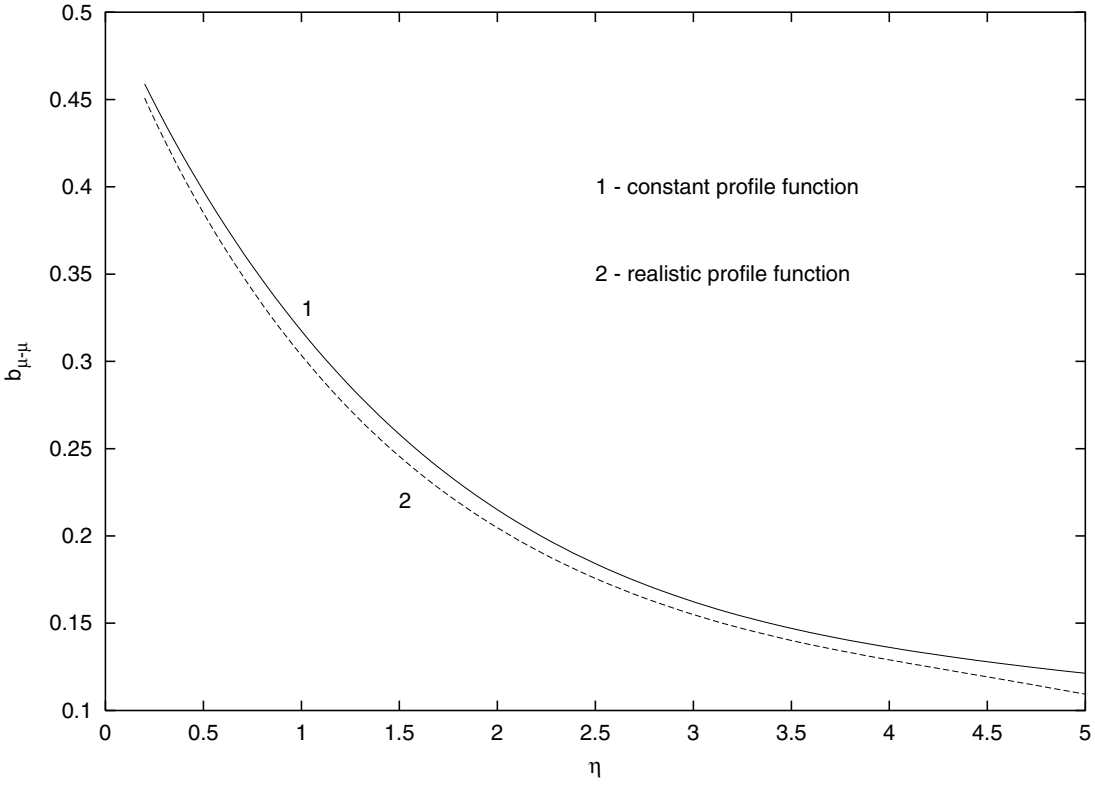

Fig. 2. Correlation coefficient $b_{\mu-\mu}$ for μ–μ correlations in the overlap scenario for the homogeneous distribution of strings and the one proportional to $T(b) \propto \sqrt{R_A^2 - b^2}$

given number of overlaps. This is clearly seen from (24) in which only the total area S_n enters and not the individual areas S_{ni}. Thus, for multiplicities all ministrings with a given overlap act coherently, as a single effective emitter. The number of these effective emitters is in fact diminished as compared to the non-interacting string case.

At $\eta \to 0$ the slope tends to its maximal value, which, as mentioned, corresponds to the independent string picture. In this case the FB correlations are wholly due to fluctuations in the total number of strings. This has to be taken into account when comparing our present results with some previous ones, where the total number of strings was fixed and as a consequence the slopes $b_{\mu-\mu}$ vanished at small η [8].

3.2 Clusters as emitters

An alternative scenario with a strong interaction between overlapping strings assumes that the color becomes homogeneously distributed over the whole cluster formed by the overlapping strings. The emitters are now clusters themselves and the index α now labels just different clusters. The average multiplicity of a cluster is chosen to adjust to the color distribution [10]:

$$\bar{m}_\alpha = \mu_0 \sqrt{\frac{n_\alpha S_\alpha}{\sigma_0}}\,, \tag{29}$$

where n_α and S_α are the number of strings and the area of cluster α. For the forward and backward rapidity window (29) transforms into

$$\bar{m}_\alpha^{\mathrm{F,B}} = \mu_0^{\mathrm{F,B}} \sqrt{\frac{n_\alpha S_\alpha}{\sigma_0}}\,. \tag{30}$$

Equations (29) and (30) express the physical contents of the cluster scenario for multiplicity correlations and their difference from (24) and (25) shows the effect of the strong interaction between overlapping strings. The remaining procedure to calculate the correlations does not change as compared to the ministring case.

We calculated the same function $F_{\mu-\mu}(x)$ (see (27)) with (29) by Monte Carlo simulations. Comparison of our results for $\langle N\rangle = 25$ and 50 again showed a satisfactory scaling in $\langle N\rangle$ for $x = 0.3 \div 3$ and a weak dependence on the way the strings are distributed in the interaction area. In spite of a very different dynamics, we have found no appreciable difference with the former case of overlaps as emitters. The slopes $b_{\mu-\mu}$ of $F_{\mu-\mu}(x)$ at $x = 1$ are shown in Fig. 1 by a long-dashed line (again for $\langle N\rangle = 50$). They are systematically higher than for overlaps but the difference does not exceed 10%, which is of no practical importance, taking into account simplifications involved at the basis of the model.

3.3 Fixed number of emitters

Technically taking the average over all geometrical distributions of strings in the transverse area is a formidable task, which can be realistically achieved by Monte Carlo simulations for a reasonable time only for a limited number of strings, substantially smaller than this number in heavy ion collisions at RHIC and especially LHC energies. On the other hand, it is well known that different ways of averaging often lead to the same or practically the same averages, since the physical picture of fluctuating variables is often basically the same. This motivates our searching for a simplified picture of string fusion, which, on the one hand, is not very different from the one discussed above by its physical implications and, on the other hand, avoids geometrical averaging. In this subsection we propose such a picture.

Physically the basis of the string fusion model consists of the appearance of various emitters homogeneously distributed in the transverse plane with the number of overlapping strings varying for 1 to N with a certain probability. One can model this physical situation by assuming a fixed number M of emitters ("cells"), each one of them (emitter α) equivalent to a certain number n_α of completely overlapped strings including $n_\alpha = 0$, in which case there is no emission at all. So effectively one also has a varying number of emitters with different colors. Averaging over configurations is achieved by distributing each n_α around some average value $\bar{n}_\alpha$ with a certain probability $P_\alpha(n_\alpha)$. The homogeneous distribution of strings in the transverse plane corresponds to equal averages: $\bar{n}_\alpha = \bar{n}$. One can model an inhomogeneous distribution of strings by distributing the M emitters in the transverse plane and choosing $\bar{n}_\alpha$ in accordance with the nuclear profile density.

In this model ("cell model" [11]) we have for the average number of particles from cell α

$$\bar{m}_\alpha = \mu_0 \sqrt{n_\alpha}, \quad \bar{m}_\alpha^{\mathrm{F,B}} = \mu_0^{\mathrm{F,B}} \sqrt{n_\alpha}\,. \tag{31}$$

If we assume that the cell probabilities $\rho_\alpha(m)$ are Poissonian, then correlations can be calculated using our formulas of Sect. 2 in exactly the same way as before. For the final averaging over configurations (that is over all n_α, $\alpha = 1, \ldots, M$) we have taken the probabilities $P_\alpha(n_\alpha)$ to be also Poissonian with a common average value $\bar{n} = \eta$ to correspond to the previous geometrical picture. Note that in this model the average value of strings is $\langle N\rangle = M\eta$.

The results of calculations of $F_{\mu-\mu}(x)$ in this model for $\langle N\rangle = 50$ and various η show that they are very close to both previous models, especially at relatively large η when they are nearly identical to those in the ministring picture. The slopes of $F_{\mu-\mu}(x)$ at $x = 1$ for the cell model are shown in Fig. 1 with a short-dashed line. So, as expected, this simplified model imitates the geometrical model of ministrings almost ideally. With that, it is much simpler: its realization by Monte Carlo simulations requires computer time more than an order of magnitude smaller than for ministrings with equal $\langle N\rangle$. Apart from this, the model admits some analytic estimates for small or large values of η, which reveal basic properties of the correlations in these asymptotical regions (see Appendix B.).

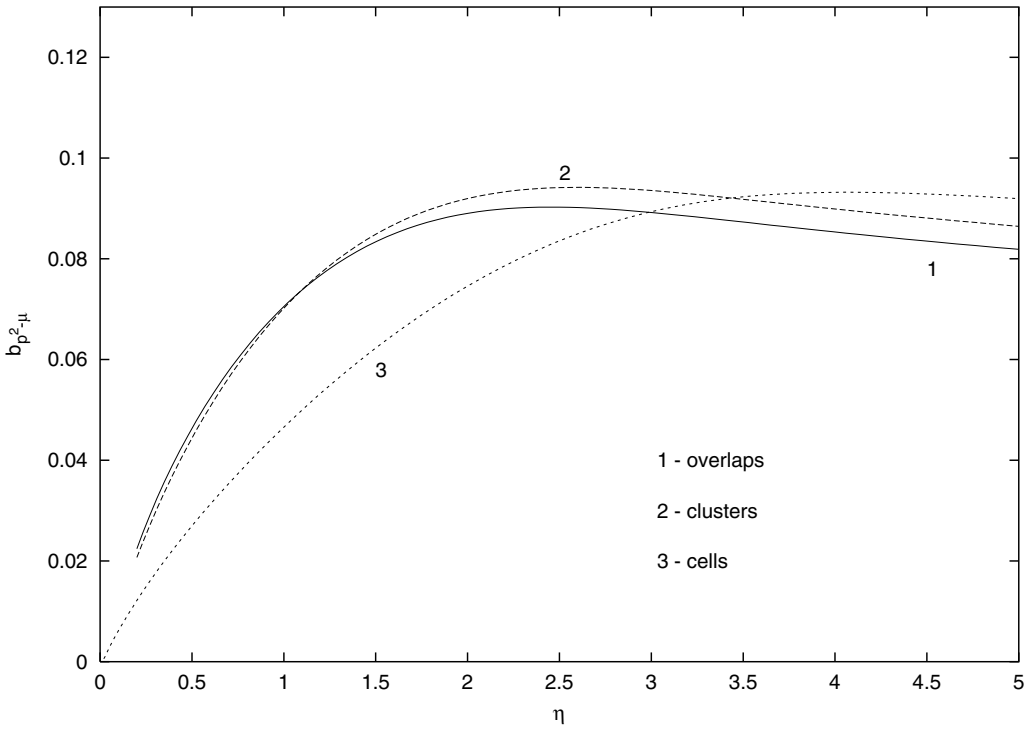

Fig. 3. Correlation coefficient $b_{p^2-\mu}$ for p^2–μ correlations in the three scenarios studied

4 Correlations between average transverse momentum and multiplicities

According to (17), to calculate the $\langle p_{\mathrm{T}}^2\rangle$–$\mu$ correlations we have to know the averages $\overline{p^2}_c$ in the backward window in a given configuration. For the Poissonian emitters they can be calculated via (21) if one knows these averages for a given emitter α (see (2)). The concrete values of p_α^2 depend on the scenario of string interaction. They were analyzed in [8,9] from where we borrow their expressions presented below.

Both for the ministring and cell scenarios the value of p_α^2 for the individual emitter are determined only by the number of strings in the overlap or cell. For ministrings

$$p_{ni}^2 = p_0^2\sqrt{n} \tag{32}$$

and for the cell model

$$p_\alpha^2 = p_0^2\sqrt{n_\alpha}\,. \tag{33}$$

For the cluster scenario p_α^2 depends on the color density inside the cluster and thus also depends on its area S_α:

$$p_\alpha^2 = p_0^2\sqrt{\frac{n_\alpha\sigma_0}{S_\alpha}}\,. \tag{34}$$

In these formulas p_0^2 is the average transverse momentum squared for the initial string.

With these expressions for p_α^2 we calculated $\langle p_{\mathrm{B}}^2\rangle_{m_{\mathrm{F}}}$ according to (17) by Monte Carlo simulations for the three scenarios considered: ministrings, clusters and cells. We studied

$$F_{p^2-\mu} = \frac{\langle p_{\mathrm{B}}^2\rangle_{m^{\mathrm{F}}}}{\langle p_{\mathrm{B}}^2\rangle} - 1\,, \tag{35}$$

considered as a function of the same variable x, (28). As before we took $\langle N\rangle = 25$ and 50 and η in the region $0.5 \div 3$. We found that $F_{p^2-\mu}(x)$ again exhibits a satisfactory scaling property: it as a result is found to be practically independent of $\langle N\rangle$. As for μ–μ correlations, $F_{p^2-\mu}(x)$ is found to be a nearly linearly rising function of x, crossing zero at $x = 1$. However, contrary to μ–μ correlations, the slopes for p^2–μ correlations rise with η. The slopes of $F_{p^2-\mu}(x)$ at $x = 1$,

$$b_{p^2-\mu} = \left(\frac{\mathrm{d}F_{p^2-\mu}(x)}{\mathrm{d}x}\right)_{x=1}\,,$$

are shown in Fig. 3 for the three studied scenarios with the homogeneous distribution of strings. One observes that the overlap and cluster scenarios again lead to practically identical results. The cell model imitates these two physical scenarios quite satisfactory at large $\eta > 2 \div 2.5$. At smaller η its slopes lie $30 \div 40\%$ below.

In contrast to the μ–μ case the slopes are now non-monotonic in η. They vanish at $\eta \to 0$, which corresponds to the absence of p^2–μ correlations for independent strings, have a broad maximum in the region of $\eta \div 1.5$–2.5 and then slowly diminish, the difference between the three scenarios becoming quite small. It is remarkable that at high η the slopes for the p^2–μ correlations become nearly equal to the slopes in the μ–μ correlations (cf. Fig. 1). This fact can be analytically derived in the cell scenario (see Appendix B).

One might be tempted to relate the maximum in the p^2–μ slopes with the percolation phase transition which takes place in the same region of η. We do not see any arguments that may support this idea. In fact the qualitative behavior of $b_{p^2-\mu}$ is the same in all three scenarios, and

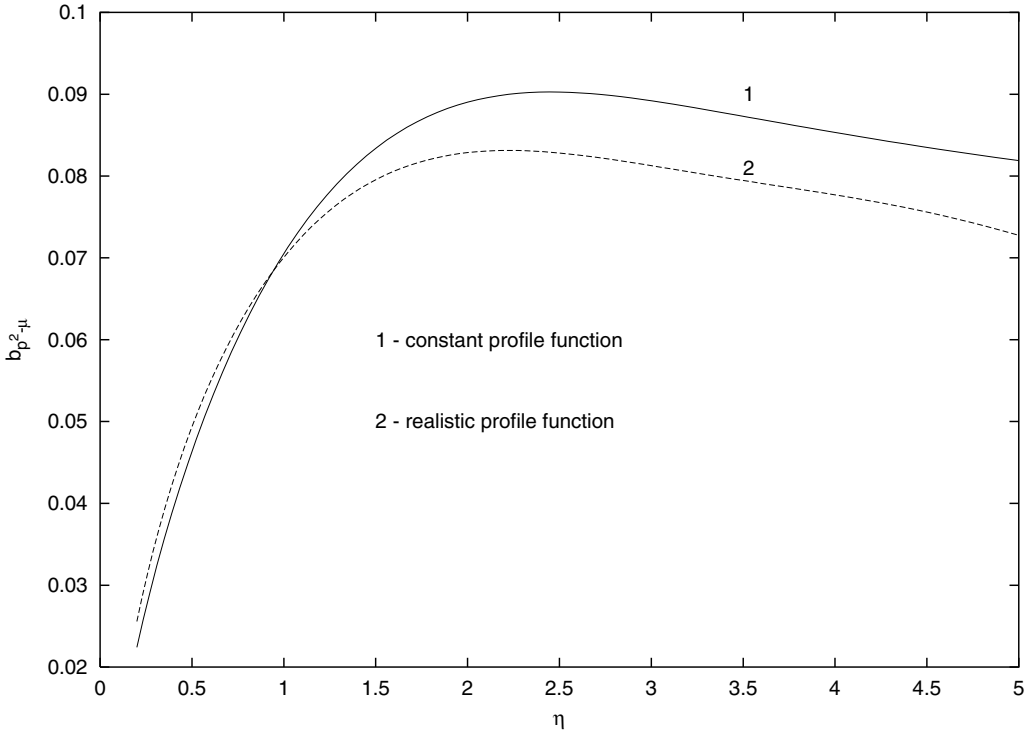

Fig. 4. Correlation coefficient $b_{p^2-\mu}$ for p^2–μ correlations in the overlap scenario for the homogeneous distribution of strings and the one proportional to $T(b) \propto \sqrt{R_A^2 - b^2}$

there is no phase transition in the cell scenario. Note that a similar behavior has been observed for dynamical transverse momentum fluctuations at RHIC, which increase at low number of participants and decrease for their number being greater than 200 [12]. This behavior can be explained in the framework of percolating strings [13], but to what extent it is related to the percolation phase transition is not clear.

In Fig. 4 we compare the slopes in the overlap scenario for the homogeneous distribution of strings and the same realistic one, as in Fig. 2. Again the difference is seen to be of little importance.

It has to be stressed that absolute values of the slopes are not too small, of the order of 0.1 in a wide range of η. Such slopes can hopefully be measured experimentally. There existence would be a clear signature of string fusion.

5 p_{B}–p_{F} correlations

The last type of correlations we shall study are those between transverse momenta of particles emitted in the forward and backward rapidity windows. They can be measured by the average transverse momenta squared of particles in the backward rapidity window at an observed transverse momentum in the forward rapidity window, (18). To calculate this in our color string model we have to know the particle spectrum $w_\alpha(p)$ for an individual emitter. This spectrum has to be chosen to lead to the averages (2), which have been discussed for each of the models for string interaction in the previous section. We choose the distribution $w_\alpha(p)$ in the form prompted by the standard fit to the experimental spectrum for the proton target [14]

$$w_\alpha(p) = \frac{(\kappa-1)(\kappa-2)}{2\pi p_\alpha^2}\left(\frac{p_\alpha}{p+p_\alpha}\right)^\kappa . \tag{36}$$

Here p_α^2 is given by (32)–(34) for the three models of string interaction considered, $p_\alpha = \sqrt{p_\alpha^2}$,

$$\kappa = 19.7 - 0.86\ln E, \quad p_0^2 = \frac{24}{(\kappa-3)(\kappa-4)}\,(\mathrm{GeV}/c)^2 , \tag{37}$$

and E is the CM energy in GeV.

With this distribution we calculated (18) for the three considered scenarios averaging over configurations by Monte Carlo simulations with a different average number of strings $\langle N\rangle = 25$ and 50. Calculations show that for these correlations the scaling function independent of $\langle N\rangle$ turns out to be

$$F_{p-p} = \langle N\rangle\left(\frac{\langle p_{\mathrm{B}}^2\rangle_{p_{\mathrm{F}}}}{\langle p_{\mathrm{B}}^2\rangle} - 1\right) . \tag{38}$$

As argument it is convenient to choose the dimensionless

$$y = \frac{p_{\mathrm{F}}}{\sqrt{\langle p_{\mathrm{F}}^2\rangle}} . \tag{39}$$

We have calculated $F_{p-p}(y)$ for different η. In all cases $F_{p-p}(y)$ is found to be a linearly rising function of y crossing zero at $y = 1$. The slopes of $F_{p-p}(y)$ at $y = 1$,

$$b_{p-p} = \left(\frac{\mathrm{d}F_{p-p}(y)}{\mathrm{d}y}\right)_{y=1} ,$$

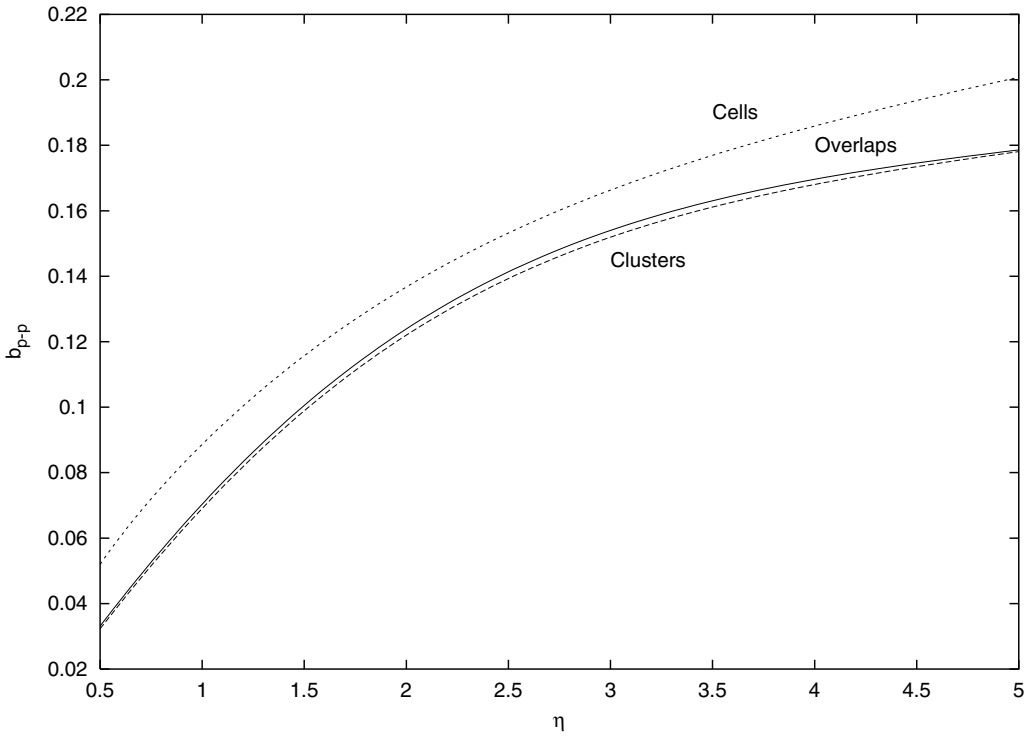

Fig. 5. Correlation coefficient b_{p-p} for p–p correlations in the three scenarios studied

are shown in Fig. 5 as functions of η for the three studied models. They rise with η similarly to the slopes in p^2–μ correlations. Again overlaps and clusters lead to practically identical results. Their imitation by cells gives rather satisfactory results, especially at $\eta > 2$, where the cell slopes lie higher than those from the other two scenarios by some 10%. At lower η this difference rises to $30 \div 40\%$.

Note that due to the presence of the factor $\langle N \rangle$ in (38) the *final* slopes for p–p correlations are given by $b_{p-p}/\langle N \rangle$. At $\eta \sim 1$ our calculated b_{p-p} are ~ 0.15. So, for realistic collisions with high $\langle N \rangle$ the magnitude of the correlations is extremely small, which excludes their experimental observation. As follows from our results, to see correlations of the order of 1% one should have $\langle N \rangle \sim 15$, which is unrealistic for $\eta > 1$.

6 Conclusions

This work was primarily motivated by the search of appropriate observables which could shed light on the details of the dynamics of color string fusion conjectured to occur in heavy ion collisions. The results of our study show that pair correlations are unfortunately rather insensitive to these details. Moreover they demonstrate that even the geometric picture of string fusion and percolation is not very essential for the found correlations. A very simplified picture, which only takes into account the existence of many emitters with different colors, leads to results not very different from the realistic geometrical overlapping of color strings. So the correlations basically reflect only the possibility of spots with a higher color field in the colliding nuclei and strongly depend only on their spatial density characterized by the parameter η.

From a certain point of view this is a positive aspect, since predictions for the correlations do not vary with specific assumptions made about the string fusion dynamics. The behavior of the correlations with η emerges as a clear signature for the basic new phenomenon characteristic for string fusion: the formation of emitters with higher color density. Both μ–μ and p^2–μ correlations look quite promising from this point of view. In particular, p^2–μ correlations arise totally due to string fusion in our picture; they are absent with independent strings. However, as mentioned in the introduction, this is only true for particles produced strictly in the central region, since in the fragmentation regions obvious p^2–μ correlations are caused by the accumulation of the string ends momenta. So, to see the effect of string fusion one should choose both rapidity windows as far as possible from the rapidity limits. As to p–p correlations, our calculations have shown that they diminish with the number of strings and appear to be negligible for realistic heavy ion collisions except at the highly peripheral collisions.

Our calculations have been made both for a homogeneous distribution of strings in the transverse interaction plane and for a realistic distribution, taking into account the varying string density as a function of the impact parameter. Our results show that the change introduced by a realistic geometry is of no practical importance.

Acknowledgements. The authors are deeply thankful to Drs. G.A. Feofilov and E.G. Ferreiro for a keen interest in this work and helpful discussions. This work was supported by the RFFI

(Russia) grant 01-02-17137 and contract FPA 2002-01161 of CICYT (Spain).

A Averages with the Poisson distribution

We start with $\rho_c(m)$ determined by (8). Presenting the Kronecker symbol as a contour integral around the origin we find

$$\rho_c(m) = \sum_{\{m_\alpha\}} \int \frac{\mathrm{d}z}{2\pi \mathrm{i} z} z^{-m+\sum_\alpha m_\alpha} \prod_\alpha \rho_\alpha(m_\alpha)\,. \quad (40)$$

We have

$$\sum_{m_\alpha} z^{m_\alpha} P(m_\alpha) = \mathrm{e}^{(z-1)\bar{m}_\alpha}\,, \quad (41)$$

so that

$$\rho_c(m) = \int \frac{\mathrm{d}z}{2\pi z^{m+1}} \mathrm{e}^{(z-1)\bar{m}_c} = \mathrm{e}^{-\bar{m}_c} \frac{\bar{m}_c^m}{m!}\,. \quad (42)$$

So we find (20).

Now take the average (7). We represent it by

$$\bar{p^2}_c = \sum_m \frac{1}{m} \sum_{\{m_\alpha\}} \prod_\alpha \rho_\alpha(m_\alpha) \delta_{m,\sum_\alpha m_\alpha} \sum_\alpha m_\alpha p_\alpha^2\,. \quad (43)$$

The internal sum over all m_α at their sum fixed can be represented in the same way as (40):

$$X \equiv \sum_{\{m_\alpha\}} \int \frac{\mathrm{d}z}{2\pi \mathrm{i} z} z^{-m+\sum_\alpha m_\alpha} \prod_\alpha \rho_\alpha(m_\alpha) \sum_\alpha m_\alpha p_\alpha^2\,. \quad (44)$$

Take some particular term in the last sum, say $\alpha = 1$ Then the sums over all m_α, $\alpha = 2, 3, \ldots, M$ will give the same factor, (41). The sum over m_1 will however contain an extra factor m_1:

$$\sum_{m_1} z^{m_1} m_1 P(m_1) = z \frac{\mathrm{d}}{\mathrm{d}z} \mathrm{e}^{(z-1)\bar{m}_1} = z\bar{m}_1 \mathrm{e}^{(z-1)\bar{m}_1}\,. \quad (45)$$

So we find

$$X = \sum_\alpha \bar{m}_\alpha p_\alpha^2 \mathrm{e}^{-\bar{m}_c} \int \frac{\mathrm{d}z}{z^{m_1}} \mathrm{e}^{z\bar{m}_c} = \frac{m}{\bar{m}_c} \rho_c(m) \sum_\alpha \bar{m}_\alpha p_\alpha^2\,, \quad (46)$$

where $\rho_c(m)$ is given by (20). Putting this into (43) we find that the factor m in (46) cancels the denominator in (43). Using then

$$\sum_m \rho(m) = 1$$

we find (21).

The derivation of (22) is done in exactly the same way.

B Analytic estimates in the cell scenario

As mentioned, the cell scenario admits explicit analytic estimates [11] valid in the limit of large or small values of η.

Estimates at large η are based on the asymptotic equivalence of the discrete Poisson distribution and continuous Gaussian distribution,

$$P_{\bar{n}}(n) \sim G_{\bar{n}}(n) = \frac{1}{\sqrt{2\pi\bar{n}}} \mathrm{e}^{-\frac{(n-\bar{n})^2}{2\bar{n}}}\,, \quad (47)$$

valid in the limit $\bar{n} >> 1$.

Let us first study the simplest case of independent strings (without fusion). Then (31) and (33) are changed to

$$\bar{m}_\alpha = \mu_0 n_\alpha, \quad p_\alpha^2 = p_0^2 \quad (48)$$

and similarly for averages in the two rapidity windows. To simplify in this appendix we shall take $\mu_0^{\mathrm{F}} = \mu_0^{\mathrm{B}}$ and denote this common multiplicity by μ_0. From the second of (48) it follows that there will be no p^2–μ correlations, as expected. The configuration averages $\bar{m}_c^{\mathrm{F,B}} = \mu_0 \sum_\alpha n_\alpha = \mu_0 N_c$ will depend only on the total number of strings N_c in a given configuration. Averaging over configuration will be reduced to averaging over the number of strings in different configurations. If the number of strings in each cell is distributed according to the Poisson distribution with average η then the total number of strings will also be distributed according to the Poisson distribution with the average $M\eta$ (see Appendix A). So at fixed η the overall average number of strings is related to M by

$$\langle N \rangle = M\eta\,. \quad (49)$$

Thus, substituting the two Poisson distributions by Gaussians we find from (16)

$$\langle m_{\mathrm{B}} \rangle_{m_{\mathrm{F}}} = \mu_0 \frac{\int_0^\infty N \mathrm{d}N\, N^{-1/2} \mathrm{e}^{-\phi(N,m_{\mathrm{F}})}}{\int_0^\infty \mathrm{d}N\, N^{-1/2} \mathrm{e}^{-\phi(N,m_{\mathrm{F}})}}\,, \quad (50)$$

where

$$\phi(N, m_{\mathrm{F}}) = \frac{(N - \langle N \rangle)^2}{2\langle N \rangle} + \frac{(m_{\mathrm{F}} - \mu_0 N)^2}{2\mu_0 N}\,. \quad (51)$$

We estimate the two integrals by the saddle point method. Then we find

$$\langle m_{\mathrm{B}} \rangle_{m_{\mathrm{F}}} = \mu_0 N_0(m_{\mathrm{F}})\,, \quad (52)$$

where N_0 is the solution of the equation $\mathrm{d}\phi/\mathrm{d}N = 0$. In terms of the scaling quantities

$$x = \frac{m_{\mathrm{F}}}{\langle m_{\mathrm{F}} \rangle}, \quad z = \frac{N}{\langle N \rangle}\,, \quad (53)$$

the equation for the saddle point takes the form

$$z^3 - z^2 = \frac{1}{2}\mu_0 (x^2 - z^2)\,. \quad (54)$$

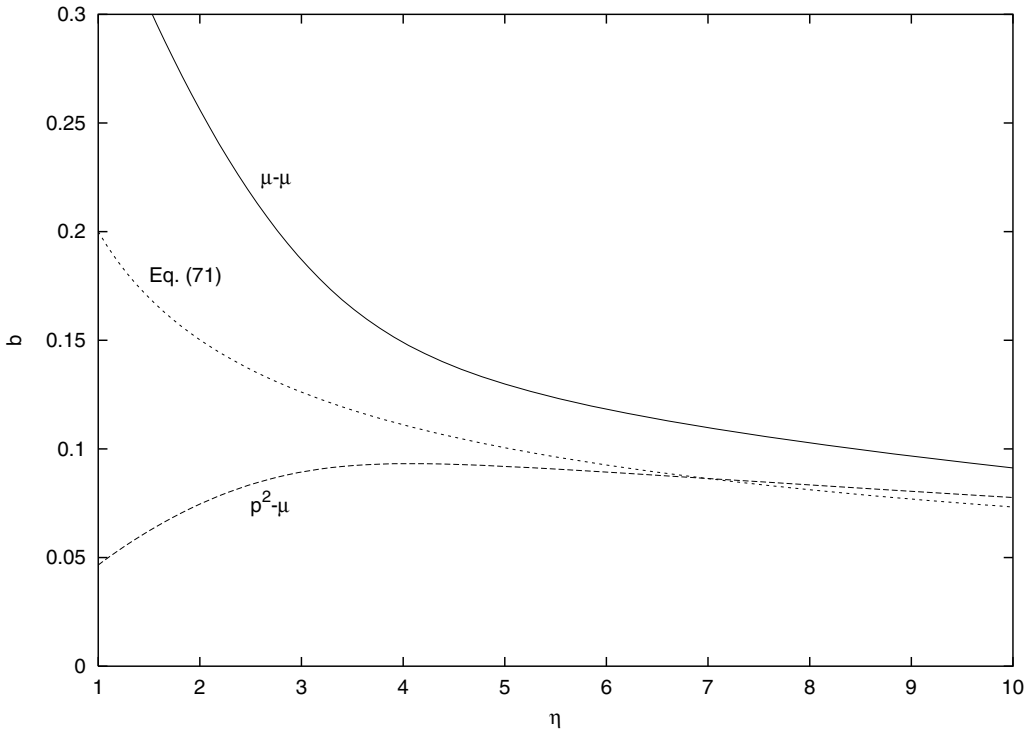

Fig. 6. Correlation coefficients for μ–μ and p^2–μ correlations in the cell model together with the asymptotics (71)

Solving this equation for $z_0(x)$ one can find the function $\langle m_{\rm B}\rangle_{m_{\rm F}}(m_{\rm F})$ at all $m_{\rm F}$. The correlation coefficient $b_{\mu-\mu}$ can however be determined explicitly from (54):

$$b_{\mu-\mu}=\left(\frac{{\rm d}z}{{\rm d}x}\right)_{x=1}=\frac{\mu_0}{\mu_0+1}\,. \tag{55}$$

Taking $\mu_0=1$ we have $b_{\mu=\mu}=0.5$ in full agreement with the limit of curves shown in Fig. 1 at $\eta\to 0$, which corresponds to independent strings.

Now we pass to the physically more interesting case when strings fuse, which in the cell scenario corresponds to (31) and (33). Introducing the quantity for a given configuration

$$r_c=\sum_\alpha\sqrt{n_\alpha}\,, \tag{56}$$

we find

$$\bar{m_c}=\mu_0 r_c,\quad \bar{p^2}_c=p_0^2\frac{N_c}{r_c}\,, \tag{57}$$

so that

$$\langle m_{\rm B}\rangle_{m_{\rm F}}=\mu_0\frac{\langle r_c P_{\mu_0 r_c}(m_f)\rangle}{\langle P_{\mu_0 r_c}(m_f)\rangle} \tag{58}$$

and

$$\langle p_{\rm B}^2\rangle_{m_{\rm F}}=p_0^2\frac{\langle (N_c/r_c) P_{\mu_0 r_c}(m_f)\rangle}{\langle P_{\mu_0 r_c}(m_f)\rangle}\,. \tag{59}$$

The average is taken over the product of Poisson distributions in n_α each with the average η.

We consider $\eta >> 1$ and substitute all Poisson distributions with Gaussian ones to get

$$\langle m_{\rm B}\rangle_{m_{\rm F}}=\mu_0\frac{\int_0^\infty\prod_\alpha {\rm d}n_\alpha r_c r_c^{-1/2}{\rm e}^{-\phi(n_\alpha,m_{\rm F})}}{\int_0^\infty\prod_\alpha {\rm d}n_\alpha r_c^{-1/2}{\rm e}^{-\phi(n_\alpha,m_{\rm F})}} \tag{60}$$

and

$$\langle p_{\rm B}^2\rangle_{m_{\rm F}}=p_0^2\frac{\int_0^\infty\prod_\alpha {\rm d}n_\alpha (N_c/r_c) r_c^{-1/2}{\rm e}^{-\phi(n_\alpha,m_{\rm F})}}{\int_0^\infty\prod_\alpha {\rm d}n_\alpha r_c^{-1/2}{\rm e}^{-\phi(n_\alpha,m_{\rm F})}}\,, \tag{61}$$

where

$$\phi(n_\alpha,m_{\rm F})=\sum_\alpha\frac{(n_\alpha-\eta)^2}{2\eta}+\frac{(m_{\rm F}-\mu_0 r_c)^2}{2\mu_0 r_c}\,. \tag{62}$$

In the saddle point approximation we find

$$\langle m_{\rm B}\rangle_{m_{\rm F}}=\mu_0 r_0,\quad \langle p_{\rm B}^2\rangle_{m_{\rm F}}=p_0^2\frac{N_0}{r_0}\,, \tag{63}$$

where N_0 and r_0 are values of N_c and r_c at the saddle point defined by the equations

$$\frac{\partial\phi(n_\alpha,m_{\rm F})}{\partial n_\alpha}=0,\quad \alpha=1,\dots,M\,. \tag{64}$$

Introducing the scaled variables

$$x=\frac{m_{\rm F}}{\langle m_{\rm F}\rangle},\quad z_\alpha=\sqrt{\frac{n_\alpha}{\eta}}\,, \tag{65}$$

and a constant involving η,

$$a=\frac{\mu_0}{4\sqrt{\eta}}\,, \tag{66}$$

we can write the saddle point equations in the form

$$z_\alpha^3-z_\alpha=a\left(x^2\frac{M^2\eta}{r_c^2}-1\right),\quad \alpha=1,\dots,M\,. \tag{67}$$

In terms of z_α here $r_c = \sqrt{\eta}\sum_\alpha z_\alpha$. Due to the symmetry in α obviously for the solution $z_\alpha = z\ z$ satisfies the single equation

$$z^3 - z = a\left(\frac{x^2}{z^2} - 1\right). \tag{68}$$

This equation defines $z = z(x)$, in terms of which one finds

$$F_{\mu-\mu}(x) = F_{p^2-\mu} = z(x) - 1\,. \tag{69}$$

So at large values of η both μ–μ and p^2–μ correlations are described by the same scaling function of x.

At $x = 1$ (68) possesses an obvious trivial solution:

$$x = 1, \quad z = 1, \ \ r_0 = M\sqrt{\eta}, \quad N_0 = \langle N\rangle = \mu_0 M\,. \tag{70}$$

This is sufficient to calculate the (identical) correlation coefficients for both μ–μ and p^2–μ correlations:

$$b_{\mu-\mu} = b_{p^2-\mu} = \frac{\mu_0}{\mu_0 + 4\sqrt{\eta}}\,. \tag{71}$$

It slowly falls with η. Of course one should have in mind that these are only asymptotic estimates, valid at sufficiently high η. To see their validity region we present in Fig. 6 the slopes b in μ–μ and p^2–μ correlations as functions of η with $\mu_0 = 1$ calculated by Monte Carlo simulations, together with the common asymptotic curve (71). As one observes, the asymptotic curve gets more or less close to the exact ones starting from $\eta > 4$–5. These are very high values from the physical point of view, attainable only at energies in the multi-TeV region for the heaviest nuclei and central collisions.

References

1. M.A. Braun, C. Pajares, Nucl. Phys. B **390**, 542, 549 (1993); N. Armesto, M.A. Braun, E.G. Ferreiro, C. Pajares, Phys. Rev. Lett. **77**, 3736 (1996); N.S. Amelin, M.A. Braun, C. Pajares, Phys. Lett. B **306**, 312 (1993); Z. Phys. C **63**, 507 (1994)
2. M.A. Braun, F. del Moral, C. Pajares, Phys. Rev. C **65**, 024907 (2002); Nucl. Phys. A **715**, 791 (2003); J. Dias de Deus, E.G. Ferreiro, C. Pajares, R. Ugoccioni, hep-ph/0304068
3. A. Capella, A. Krzywicki, Phys. Rev. D **29**, 1007 (1984); P. Aurenche, F. Bopp, J. Ranft, Phys. Lett. B **147**, 212 (1984); A. Capella, J. Tran Thanh Van, J. Kwiecinski, Phys. Rev. Lett. **58**, 2015 (1987)
4. I. Derado et al., Z. Phys. C **40**, 25 (1988)
5. A. Capella, J. Tran Thanh Van, Phys. Rev. D **29**, 2512 (1984)
6. T.T. Chou, C.N. Yang, Phys. Lett. B **135**, 175 (1984); Phys. Rev. D **32**, 1692 (1985); M.A. Braun, C. Pajares, V.V. Vechernin, Phys. Lett. B **493**, 54 (2000)
7. N.S. Amelin, N. Armesto, M.A. Braun, E.G. Ferreiro, C. Pajares, Phys. Rev. Lett. **73**, 2813 (1994)
8. M.A. Braun, C. Pajares, Eur. Phys. J. C **16**, 349 (2000)
9. A. Rodrigues, R. Uggocioni, J. Dias de Deus. Phys. Lett. B **458**, 402 (1999)
10. M.A. Braun, F. del Moral, C. Pajares, Eur. Phys. J. C **21**, 557 (2001)
11. V.V. Vechernin, R.S. Kolevatov, hep-ph/0304295; hep-ph/0305136
12. J. Nystram et al., PHENIX collaboration, Nucl. Phys. A **715**, 603c (2002)
13. E.G. Ferreiro, F. del Moral, C. Pajares, hep-ph/0303137; J. Dias de Deus, A. Rodrigues, hep-ph/0308011
14. M.A. Braun, C. Pajares, Phys. Rev. Lett. **85**, 4864 (2000)